NJC

Accepted Manuscript

This article can be cited before page numbers have been issued, to do this please use: H. Zheng, C. Wang, X. Zhang, L. Kong, Y. Li, Y. Liu and Y. Liu, *New J. Chem.*, 2016, DOI: 10.1039/C5NJ02981C.

View Article Online
DOI: 10.1039/C5NJ02981C

Ultrasonic spray pyrolysis assembly of TiO_2-WO_3-Pt multi-heterojunction microspheres photocatalyst by highly crystallized WO_3 nanosheet: less is better

Han Zheng,[1**] Changhua Wang,[1,2**] Xintong Zhang,[1*] Lina Kong,[1] Yingying Li,[1] Yunyu Liu,[3] Yichun Liu[1]

[1]Center for Advanced Optoelectronic Materials Research, and Key Laboratory of UV-Emitting Materials and Technology of Ministry of Education, Northeast Normal University, 5268 Renmin Street, Changchun 130024, China
[2]College of Chemistry and Biology, Beihua University, Jilin 132103, China
[3]College of Chemistry, Northeast Normal University, 5268 Renmin Street, Changchun 130024, China

Abstract: Multi-heterojunction is more promising than single-heterojunction in photocatalysis due to the availability of more interfaces between each component. However, its photocatalytic activity is highly dependent on the contact mode of individual component. In this work, we assemble TiO_2-WO_3-Pt multi-heterojunction microspheres by ultrasonic spray pyrolysis and focus on their contact mode governed photocatalytic activity. The results reveal that highly crystalline WO_3 nanosheets as building blocks could particularly enhance the photocatalytic activity of TiO_2/WO_3 system toward degrading gaseous acetaldehyde and isopropyl alcohol. Furthermore, loading of Pt nanoparticles on WO_3 nanosheets could facilitate to a more prominent enhancement of activity than that of TiO_2/Pt, benefiting from the two-electron reduction of oxygen at the interface of WO_3/Pt. Meanwhile, high crystallinity of WO_3 nanosheets allows a loading amount of Pt as low as 0.04 wt% in TiO_2-WO_3-Pt system, which reduces the catalyst cost in comparison with the conventional amount of 1wt%.

1. Introduction

TiO_2 continues to gain research interest in photocatalysis-related

* Corresponding author. Tel./Fax: +86 431 85099772; E-mail: xtzhang@nenu.edu.cn
** These authors contributed equally to the work.

View Article Online
DOI: 10.1039/C5NJ02981C

applications.[1-4] Recent study reveals that its solar conversion efficiency could be further improved when TiO_2 meets second metal oxide in terms of type II heterojunction.[5-15] For example, Zhang et al.[14] prepared the WO_3/TiO_2 composites and 5.0% WO_3/TiO_2 composite showed far superior photoactivity as compared to pure TiO_2, P-25 and pure WO_3 in the degradation of methyl orange and 2,4-dichlorophenol in UV and visible light. Liu et al.[15] developed Bi_2MoO_6 nanosheet/TiO_2 nanobelt heterostructure and observed an excellent photodegradation performance under UV and visible light irradiation. Moreover, such a heterostructure possessed high photocatalytic oxygen production with a rate of 0.668 mmol h^{-1} g^{-1}. However, among part of type II heterojunctions, conduction band of secondary oxide in type II heterojunction is lower than that of TiO_2 and thereby photogenerated electrons on the side of secondary oxide are difficult for onset of single-electron reduction of oxygen. As such, photo-generated electrons flowed from TiO_2 to foreign component across interface of heterojunction usually tend to seriously aggregate on the side of secondary metal oxide and result in unfavorable "back electron transfer" recombination.

To overcome the difficulty in initiation of oxygen reduction by photo-generated electrons, promotion of multi-electron transfer is found to be an alternative mean in order to boost the photocatalytic activity of aforementioned metal oxides.[16-18] For example, the potential of conduction band of Ag_3PO_4 cannot match the redox potentials of single-electron reduction of oxygen. However, the two-electron reduction of oxygen over Ag_3PO_4 can be initiated and result in remarkable photooxidation ability.[19] Similarly, Abe et al. [20] reported that Pt-WO_3 photocatalytically decomposed isopropyl alcohol with ca. 100-fold enhanced CO_2 generation rate, while only 4-fold enhancement was observed for Pt-(N-TiO_2). The reason for high activity of Pt-WO_3 was due to the promotion of multi-electron reduction of O_2 on the Pt cocatalyst rather than single-electron reduction. Hashimoto et al. grafted Cu(II) or Fe(III) species on a series of oxides, such as $Ti_{1-3x}W_xGa_{2x}O_2$,[21] $(Sr_{1-y}Na_y)(Ti_{1-x}Mo_x)O_3$, [22] Ti^{3+} self-doped TiO_2 [23] and Fe doped TiO_2. [24] The grafted species consistently enhance photocatalytic activity toward degradation of isopropyl

View Article Online
DOI: 10.1039/C5NJ02981C

alcohol induced by interfacial charge transfer (IFCT) process and thereafter consumption in multi-electron reduction of O_2 mediated by the surface clusters.

On the basis of above considerations, integration of advantages of type II heterojunction (wide light absorption range and improved charge separation) and cocatalyst (multi-electron induced surface reaction) into multi-heterojunction becomes a very promising way to access to high solar conversion efficiency. With regard to multi-heterojunction, contact mode between individual components is highly critical. For instance, Hoffmann et al. observed high hydrogen production rate about (6-9) $\times 10^{-3}$ mol h^{-1} g^{-1} over CdS/(Pt-TiO_2), which is higher by a factor of 3-30 than that of Pt-(CdS/TiO_2).[25] Wang et al. showed a synergistic enhancement of H_2 evolution over the Pt/SnO_x/TiO_2 heterostructures formed by anchoring Pt NPs at SnO_x sites, whereas the rate of H_2 evolution over Pt/TiO_2/SnO_x counterparts prepared by grafting SnO_x species on Pt/TiO_2 was significantly decreased.[26] Pap et al.[27] obtained TiO_2/WO_3/noble metal (Au or Pt) composites by means of selective photodeposition of noble metal on desired surface of TiO_2 or WO_3. Major differences were observed in photocatalytic activity toward degradation of oxalic acid and production of hydrogen over catalysts wherein only the position of the noble metal was changed. We have fabricated (WO_3-Pt)/TiO_2 multi-heterojunction photocatalyst based on WO_3 nanorods and Pt and TiO_2 nanoparticles.[28] The photocatalytic performance of the multi-heterojunction under visible light was found dependent on the location of the loaded Pt nanoparticles. Pt surface loading on WO_3, as opposed to loading on the TiO_2 surface, was more beneficial in maximizing the photocatalytic activity. Therefore, contact mode of chosen building blocks should not be overlooked and multiheterojunction should be smartly designed for photocatalysis.

Inspired by these reports, in this work, we continue to focus on multi-heterojunction assembled from TiO_2, WO_3 and Pt as well as their contact mode dependent photocatalytic activities. Furthermore, ultrasonic spray pyrolysis technique is employed to assemble multi-heterojunction due to fact that production of porous microspheres where light trapping via multiple scattering at air-solid interface is favored. Highly crystallized WO_3 nanosheets are chosen as building blocks for the

View Article Online
DOI: 10.1039/C5NJ02981C

sake of not only good contact with TiO_2 and Pt nanoparticles but also minimization of defects at the interface. Structural features and photocatalytic activities of as-assembled multi-heterojunction will be systematically discussed.

2. Experimental Section

2.1 Materials and Characterization

2.1.1 Materials

TiO_2 powders (Degussa P25) were obtained from Nihon Aerisol Co. $H_2PtCl_6 \cdot 6H_2O$ was purchased from Aladdin in analytical grade purity. Acetaldehyde (2 vol% in N_2) and CO_2 (2 vol% in N_2) were obtained from Beijing Chemical Co. Bi_2O_3, WO_3 powders were purchased in analytical purity from Chinese National Medicine Group Chemical Reagent Co. All chemical reagents were used as received, without further purification.

2.1.2 Preparation of WO_3 nanosheets

WO_3 nanosheets were synthesized by stoichiometric amounts of Bi_2O_3 and WO_3 to 800 ℃ for 16 h. The obtained powders were ground and then treated with 6M HCl solution for 3 days at room temperature to promote the proton exchange. The obtained light yellow suspension was centrifuged, washed thoroughly with deionized water to remove the residual acid, and finally dried at 80 ^oC in air overnight. The obtained powders(0.4 g) was immersed into 100 ml tetramethylammonium hydroxide aqueous solution (0.0028 M) for 8 days with continues stirring. As a result, a colloidal suspension with a light green appearance was obtained successfully, as references [29]. After centrifugation and drying at 80 ^oC, the obtained products were WO_3 nanosheets.

2.1.3 Preparation of WO_3/Pt hybrids

The WO_3 nanosheet sample (100 mg) was added into 10 ml water and ultrasonically dispersed for 10 min, and then, aqueous H_2PtCl_6 solution (256μl , 0.1 M) and 1.1 mL methanol was added. The solution was stirred continuously under UV light (340-420 nm) irradiation for 2 h.[30] The as-obtained Pt-loaded WO_3 nanosheets were centrifuged and dried at 343 K at ambient condition. The stoichiometric ratio of Pt on WO_3 is 1 wt%.

View Article Online
DOI: 10.1039/C5NJ02981C

2.1.4 Preparation of TiO_2-WO_3-Pt multi-heterojunction

TiO_2-WO_3-Pt microspheres were prepared by the ultrasonic spray pyrolysis method. Typically, P25 TiO_2 powders (3 g) and pre-synthesized WO_3-Pt composite (0.12 g) were dispersed into 1000 ml of water to form a mixture suspension. Subsequently, the suspension was atomized by an ultrasonic nebulizer, and the formed mist was passed through a quartz tube heated at 1073 K. Then, powders were collected at an electrostatic collecting device connected to the end of the quartz tube. Finally, the as-obtained powders were annealed at 773 K for 30 min under ambient conditions.

2.1.5 Characterization

X-ray diffraction (XRD) characterization was carried out on a Rigaku D/max-2500 X-ray diffractometer. Photoluminescence (PL) spectra were recorded on a Jobin-Yvon HR800 instrument with an Ar^+ laser source of 325 nm wavelength in a macroscopic configuration. Morphology and composition analyses were carried out on a FEI quanta 250 field emission scanning electron microscopy (FESEM) and a high resolution electronic micrographs were acquired using a JEOL JEM-2100 transmission electron microscope (TEM) operated at an acceleration voltage of 200 kV. UV-Vis diffusion reflectance (DR) spectra were recorded on a Lambda 900 UV–vis–NIR spectrophotometer, using $BaSO_4$ as reference.

2.1.6 Photocatalytic Test

Photocatalytic properties of samples were investigated by measuring the photodegradation of gaseous acetaldehyde and isopropanol under solar light irradiation. 0.05 g microsphere powders were uniformly spread in a sample holder with a geometric area of 0.25 cm^{-2}, which was placed on the bottom of a 500 mL cylinder-type Pyrex glass vessel. The glass vessel was flushed with O_2 (20%)/N_2 gas to remove carbon dioxide from the system, and the relative humidity of atmosphere inside the vessel was controlled to 45% by passing the O_2/N_2 gas through chilled water. 5 mL acetaldehyde was introduced into the reaction vessel using a

View Article Online
DOI: 10.1039/C5NJ02981C

Pressure-Lock syringe to reach a concentration of 200 ppmv. After keeping dark for 30 min, the glass vessel was irradiated from top by a 150 W xenon lamp (Hayashi UV410) which emit light of wavelength range of 350-700 nm. The light intensity irradiated on the samples was determined to be 1 mW/cm^2 at 365 nm by light intensity meter from Beijing Normal University. The degradation of acetaldehyde and the generation of carbon dioxide were monitored using a gas chromatograph (SP-2100A, BFRL Co.), equipped with a 2 m Porapak-Q column and a flame ionization detector. Isopropanol and acetone were monitored on gas chromatograph (GC2014C，SHIMADZU Co.), equipped with a WonderCap Wax column and a flame ionization detector.

3. Results and Discussion

In our work, firstly, we synthesize highly crystalline WO_3 nanosheet, employ photochemical method to load platinum (Pt) on the WO_3 nanosheet to form a noble metal-semiconductor heterostructure. The reason to choose highly crystalline WO_3 nanosheets instead of traditional WO_3 nanopaticles is that highly crystalline WO_3 nanosheet has few defects and inhibits recombination of electrons and holes. In addition, lamellar material has more reaction sites which are helpful for forming a good contact between Pt nanoparticles and WO_3 nanosheets. Subsequently，we combine pure TiO_2 (P25) with Pt loaded WO_3 nanosheets to form multi-heterojunction microspheres with ordered contact by a ultrasonic spray pyrolysis method. The multi-heterojunction microspheres microspheres have follow advantages：(1) porous microspheres are facile for adsorption of organic compounds and improve the photocatalytic activity due to their large surface areas. (2) The multiple heterogeneous structure photocatalyst with ordering contact mode can migrate the photogenerated electron and holes and suppress recombination more effectively than pure TiO_2 and TiO_2-WO_3 binary-heterogeneous structure. (3) Only rarely little platinum nanoparticles (0.04%，relative to the amount of TiO_2) are loaded in the multiple heterostructure photocatalyst, which not only results in activity enhancement but also save cost in comparison with traditional value of 1%.

View Article Online
DOI: 10.1039/C5NJ02981C

3.1 Structure and morphology

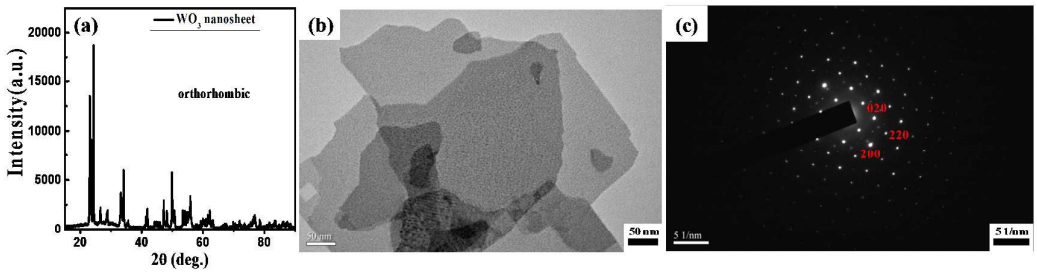

Fig.1: Structural characterization of WO_3 nanosheets: (a) XRD pattern; (b) TEM image; (c) SAED pattern.

XRD and HRTEM analysis are performed to characterize pre-synthesized WO_3 nanosheets. As shown in Fig.1a, all diffraction patterns can be well indexed to orthorhombic phase (JCPDS No.20-1324). TEM image in Fig. 1b shows that the products are nanosheets with side length of ca. 400 nm. In HRTEM image (Fig. 1c) of a WO_3 crystallite, interplanar distances corresponding to d(020) (0.384 nm measured; 0.3783 nm theoretical) and d(002) (0.392 nm measured, 0.3894 nm theoretical) are separated by a 89.6° ± 0.5° measured angle (90° theoretical). Corresponding selected area diffraction pattern shows a typical orthorhombic symmetry consisting of clear spots with strong diffraction, indicating the high crystallinity of WO_3 nanosheet. The clear spots can be labeled with planes of (002), (200) and (220) of orthorhombic WO_3, respectively.

SEM images of different samples synthesized by ultrasonic spray pyrolysis are shown in Fig. 2. As can be seen in Fig. 2a, pristine TiO_2 samples display the morphology of polydispersed microspheres with diameters from 0.5 to 2 μm. The surface of the spheres is not smooth, suggesting that the resulting microspheres are formed by the aggregation of nanoparticles driven by the drying of mist droplets. Similar phenomenon has been observed in ultrasonic spray pyrolysis prepared microspheres such as TiO_2, [31] Fe_2O_3, [32] ZnS [33] and SiO_2. [34] On the contrary, pure WO_3 samples in Fig. 2d show broken and hollow spheres with smooth surface, probably resulting from the difficult agglomeration of the primary large-sized nanosheets. After incorporating WO_3 nanosheets or WO_3/Pt hybrids with TiO_2 nanoparticles, porous

View Article Online
DOI: 10.1039/C5NJ02981C

microspheres can be well maintained as shown in Fig. 2b and c. The edges of WO_3 nanosheets can not be distinguished in the microspheres, mainly due to their tendency of curling or wrapping in TiO_2 nanoparticles.

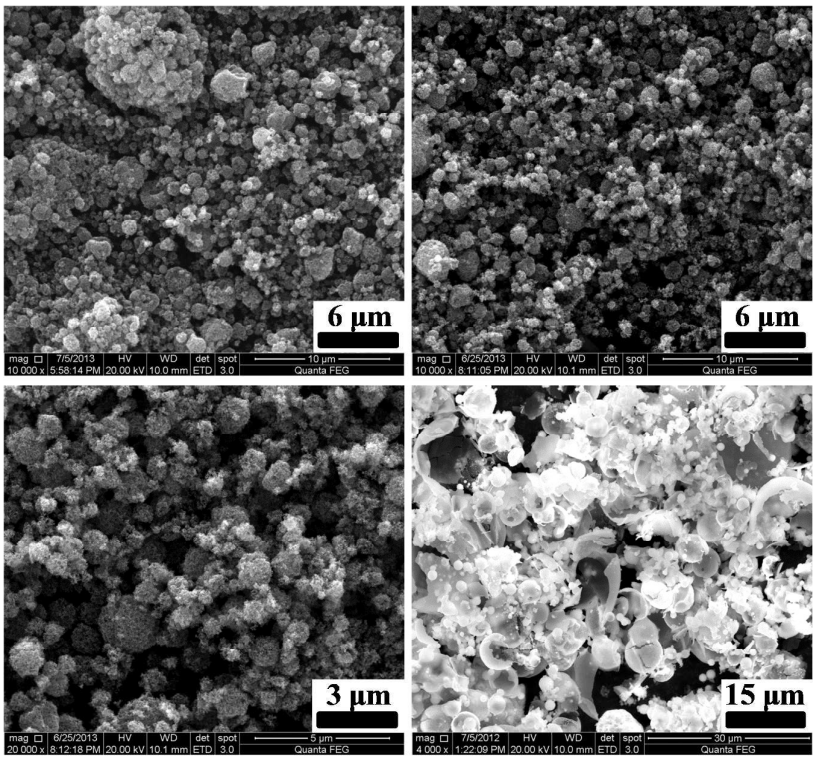

Fig.2: SEM images of (a) pristine TiO_2, (b) TiO_2/WO_3, (c) TiO_2-WO_3-Pt and (d) WO_3 samples

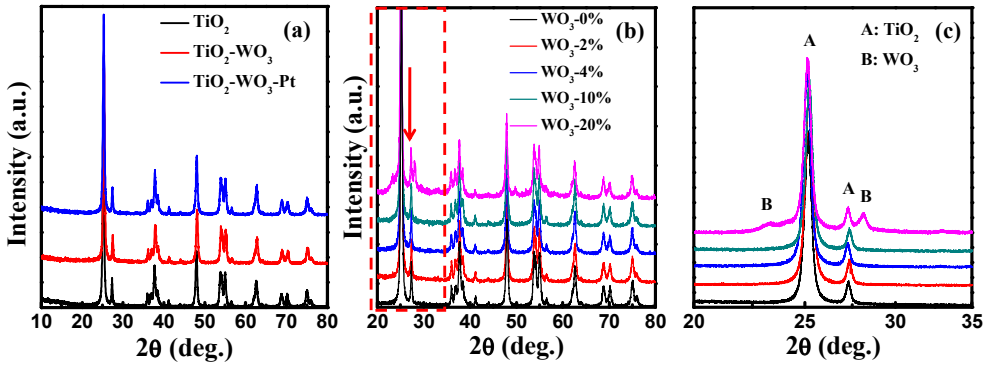

Fig.3: (a) XRD patterns of pure TiO_2, typical TiO_2-WO_3 and TiO_2-WO_3-Pt samples; (b and c) XRD patterns of different TiO_2-WO_3-Pt multi-heterojunctions and enlargement of the region between 20-35 degrees.

View Article Online
DOI: 10.1039/C5NJ02981C

Fig. 3 depicts XRD patterns for the samples prepared by ultrasonic spray pyrolysis. For pure TiO_2, diffraction peaks (Fig. 3a) at 2θ = 25.22°, 37.78°, 47.94°, 54.96°, and 62.69° can be respectively indexed to the (101), (004), (200), (211), and (204) planes of anatase (JCPDS No. 21-1271). In addition, diffraction peaks attributed to rutile are found, as shown by the appearance of its (110) reflection at ~27.4° of 2θ (JCPDS No. 21-1276). There is no any other characteristic peak in the XRD patterns, which confirms that other new phases are not formed during the preparation processes. Hence, the crystalline structure of pure TiO_2 is the mixture of anatase and rutile phase. For the WO_3-TiO_2-Pt composites, no diffraction peaks of WO_3 can be found until the content of WO_3 reaches 20 wt% (Fig.3b and c), resulting from either the low amount or high dispersity of WO_3 component on TiO_2. In curve Fig.3b and c, as-detected diffraction peaks located at 23.70° and 28.77° can be attributed to orthorhombic phase of WO_3 (JCPDS No. 20-1324). No diffraction peaks of noble metal Pt are detected in all TiO_2-WO_3-Pt samples, which is mainly due to the ultra-small size of Pt nanoparticles and their quite low amount.

The structure of the as-prepared heterojunctions was further studied by TEM and HRTEM. Fig.4a shows the HRTEM for platinum loaded WO_3 nanosheet samples. It is shown that Pt nanoparticles have a close contact to WO_3 nanosheet and WO_3/Pt heterostructure is well formed. In typical TEM image of WO_3-TiO_2-Pt microspheres shown in Fig. 4b, uniform distribution of pores in microspheres is once again observed, confirming above observation in SEM images. HRTEM image (Fig. 4c) clearly shows an interface between WO_3 and TiO_2. The fringe spacing of 3.545 Å and 2.63 Å can be indexed to (101) plane of anatase TiO_2, and (220) plane of orthorhombic WO_3, respectively.

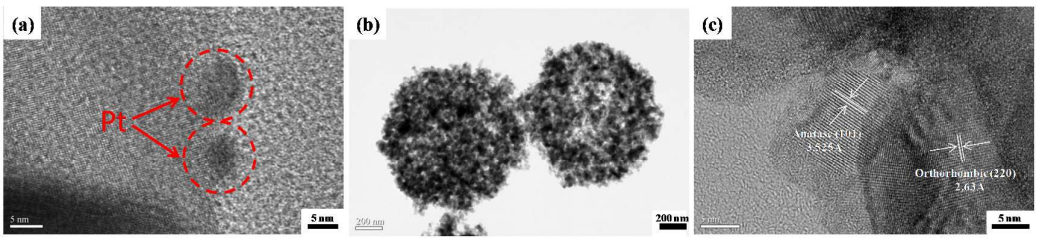

Fig. 4: (a) HRTEM image of WO_3-Pt heterojunction, (b,c) TEM and HRTEM images of TiO_2-WO_3-Pt multi-heterojunction microspheres.

View Article Online
DOI: 10.1039/C5NJ02981C

3.2 Optical properties

Fig. 5 depicts the typical diffuse reflectance spectra of pure-TiO_2, TiO_2-WO_3 and TiO_2-WO_3-Pt. All spectra are dominated by the edge due to the O^{2-}-Ti^{4+} charge transition in anatase TiO_2 at 300-380 nm, which is comparable to the excitation of electrons from the valence band to the conduction band. UV-vis spectra performed in the diffuse reflectance mode (R) are transformed to the Kubelka-Munk function F(R) to separate the extent of light absorption from scattering. The value of band gap is obtained from the plot of the Kubelka–Munk function $(F(R)E)^{1/2}$ versus the energy of the absorbed light E. Accordingly, the band gap (Eg) for pure TiO_2 is calculated to be ca. 3.07 eV, which fall within the range of mixed phases of anatase and rutile. Different from previously reported TiO_2-WO_3 composites, no red-shift of the absorption edge of TiO_2-WO_3 and TiO_2-WO_3-Pt in comparison with pristine TiO_2 is observed, mainly resulting from the low content of WO_3 and its high dispersion in the composite. [31,35] Hence, it can be deduced that as-incorporated WO_3 components in multi-heterojunction have no influence on the absorption properties of TiO_2. In other words, in spite of narrower band gap of WO_3 than that of TiO_2, the photocatalytic activity of either TiO_2-WO_3 or TiO_2-WO_3-Pt may not be influenced by means of improvement of absorption property.

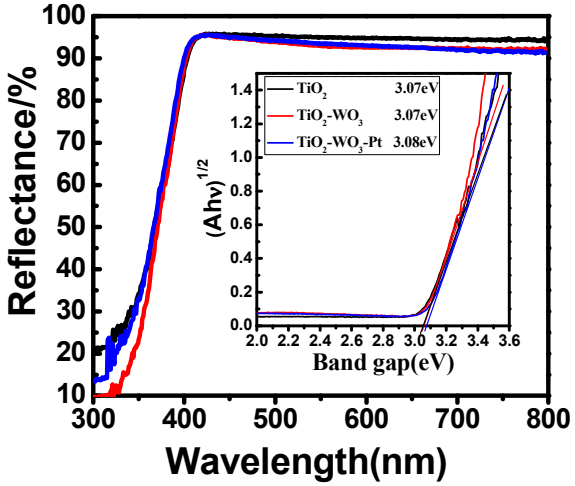

Fig.5: UV-Vis-DRS spectra of different samples

Photoluminescence (PL) spectroscopy has been useful in the field of photocatalysis.[36-39] Information such as surface oxygen vacancies and defects, as well

View Article Online
DOI: 10.1039/C5NJ02981C

as the efficiency of charge carrier trapping, immigration and transfer can be obtained. For pure TiO_2, as illustrated in Fig. 6, it exhibits a broad emission band in the visible light region. It is believed that the peaks result from the electronic transition mediated by the defect levels such as oxygen vacancies in the band gap.[40] After incorporating with WO_3 nanosheets, the intensity of TiO_2 is significantly decreased. Considering that the PL emission is the result from the free charge carrier recombination, the lower PL intensity indicate that the TiO_2-WO_3 photocatalyst has a lower recombination rate of photo-generated electrons and holes,[41] which is due to the fact that the electrons and holes are separated by the charge transfer at the heterojunction interfaces of WO_3 nanosheets and TiO_2 nanoparticles. More importantly, TiO_2-WO_3-Pt multi-heterojunction shows drastic quenching of PL intensity, suggesting a markedly enhanced charge separation co-promoted by WO_3/Pt and WO_3/TiO_2 heterojunction. This result confirms significant participations of WO_3 nanosheets and WO_3/Pt heterojunction in the decrease of recombination of photo-generated electron-hole pairs.

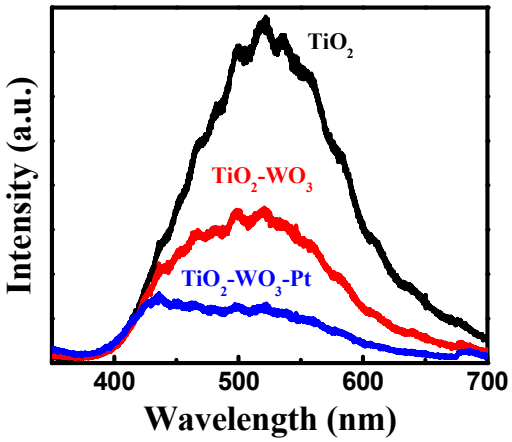

Fig.6: PL spectra of different samples

3.3 Photocatalytic performance

The photocatalytic test was investigated against degradation of acetaldehyde under solar light with intensity of 1 mw/cm^{-2} at 365 nm. For comparison, TiO_2-Pt (the same method of photochemical Pt loading, the quantity of Pt is 0.04 wt % relative to the entire photocatalyst microspheres) were also fabricated by ultrasonic spray pyrolysis method. Fig. 7a,b shows typical plots of decrease of acetaldehyde and

View Article Online
DOI: 10.1039/C5NJ02981C

increase of CO_2 concentration as a function of irradiation time on different photocatalysts. According to the Langmuir-Hinshelwood kinetics model, the apparent rate for acetaldehyde degradation can be expressed as:

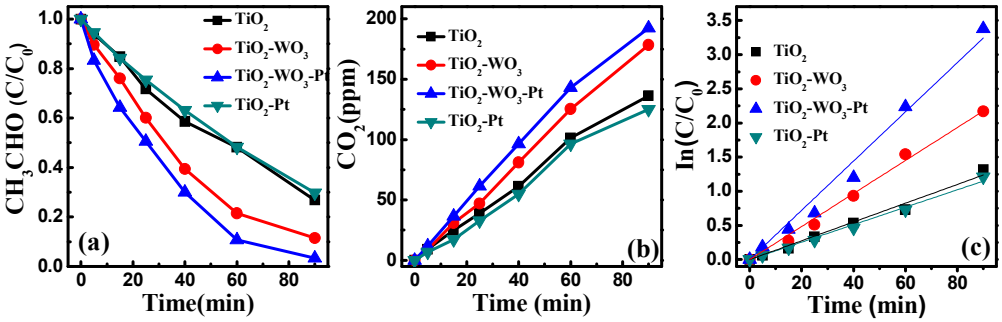

Fig.7: (a) Degradation curves of acetaldehyde over different samples, (b) CO_2 evolution curves over different samples, (c) reaction kinetic curves over different samples.

$\ln(C_0/C) = kt$, where C is the concentration of acetaldehyde during photocatalytic reaction, t is the reaction time, and C_0 is the initial concentration of acetaldehyde. The apparent first order rate constant, k, are given by the slope of $\ln(C_0/C)$ versus t, and the results are 0.01422, 0.01325, 0.02491 and 0.0379 min^{-1} for TiO_2, TiO_2-Pt, TiO_2-WO_3 and TiO_2-WO_3-Pt microspheres, respectively (Fig.7c). For TiO_2-WO_3 photocatalyst, it is more efficient in degradation of acetaldehyde than that of pure TiO_2, which agrees well with previous TiO_2-WO_3 system. Notably, loading of Pt nanoparticles on the surface of P25 hardly exhibits improvement of activity in terms of either decrease rate of acetaldehyde or evolution rate of CO_2. Different from most study of TiO_2/Pt photocatalyst, our results suggest a poor improvement of the photocatalytic activity of TiO_2 after Pt loading, which is mainly due to the very few amount of Pt loading as low as 0.04%. Interestingly, when the same amount of Pt is loaded on WO_3, as-obtained TiO_2-WO_3-Pt multi-heterojunction displays a dramatic decrease of acetaldehyde and increase of CO_2 concentration at initial 60 min. About 90% of acetaldehyde was oxidized into CO_2 after 60 min, showing the most excellent photocatalytic activity of TiO_2-WO_3-Pt multi-heterojunction. Herein, it should be noted that Pt loading percentage in previous Pt/metal oxide composite photocatalyst is

View Article Online
DOI: 10.1039/C5NJ02981C

usually 1% in most reported results. In our case, the significant enhancement of activity induced by incorporation of less amount of Pt of 0.04% in multi-heterojunction can be explained as following: Pt nanoparticles are in-situ photodeposited on the surface of WO_3 nanosheets. As demonstrated in aforementioned XRD and HRTEM results, WO_3 nanosheets are highly crystallized. Under UV light irradiation, high crystallization of WO_3 nanosheets can ensure easy immigration of photo-excited electrons from crystal inner to surface, less trapping of electrons by surface defects states and inhibition of recombination of electrons and holes. As such, H_2PtCl_6 is effectively photoreduced by electrons on the surface of WO_3 nanosheets and hence Pt nanoparticles are uniformly deposited on WO_3 surface without aggregation. Therefore, WO_3/Pt interface with high amount and good quality are produced, even if the Pt loading amount is lower than conventional value of 1%. Benefiting from the electrons flowing from WO_3 to Pt and onset of multi-electron reduced of oxygen, the photocatalytic performance of multi-heterojunction is obviously boosted.

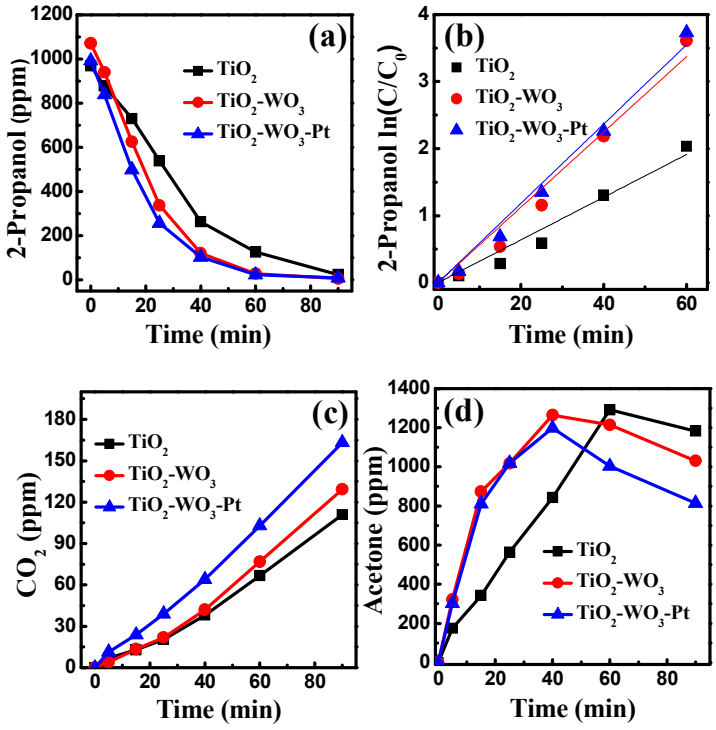

Fig. 8: (a) Degradation curves of isopropanol over different samples, (b) reaction kinetic curves over different samples, (c) CO_2 evolution curves over different samples, (d) concentration curves of acetone intermediate over different samples.

View Article Online
DOI: 10.1039/C5NJ02981C

Meanwhile, isopropanol was also employed as substance to further verify above photocatalytic results.[42,43] It is well known that the photocatalytic decomposition of isopropanol proceeds via formation of acetone as an intermediate followed by further decomposition of acetone to the final products CO_2 and H_2O. Fig.8 shows time courses of the concentration of products generated from 2-propanol over TiO_2, TiO_2-WO_3 and TiO_2-WO_3-Pt under solar light irradiation. For bare TiO_2, either generation rate of acetone intermediate or evolution rate of CO_2 is slower than that of TiO_2-WO_3 and TiO_2-WO_3-Pt samples, suggesting the less efficiency of TiO_2 in degradation of isopropanol (Fig. 8a-d). For TiO_2-WO_3 and TiO_2, the higher amount of acetone intermediate and lower evolution rate of CO_2 at the late stage indicate their insufficient oxidation ability. For TiO_2-WO_3-Pt multi-heterojunction, it shows a comparable generation rate of acetone to that of TiO_2-WO_3 at the initial 40 mins, and whereas a slower rate to that of TiO_2-WO_3 at the last 40 mins (Fig. 8d). Importantly, TiO_2-WO_3-Pt multi-heterojunction displays higher evolution rate of CO_2 than that of TiO_2 and TiO_2-WO_3 during the whole photocatalytic reaction (Fig. 8c). In this regard, it can be deduced that TiO_2-WO_3-Pt multi-heterojunction is highly active for both oxidation of isopropanol to acetone and further mineralization of acetone to CO_2. Therefore, in combination with the photocatalytic results of degradation of acetaldehyde and isopropanol, it is safe to conclude that TiO_2-WO_3-Pt multi-heterojunction sample displays superior photocatalytic activity to that of pure TiO_2 and TiO_2-WO_3.

Mechanism for the enhancement of photocatalytic activity of the TiO_2-WO_3-Pt can be explained by Scheme 1. Since the conduction band edge of WO_3 is lower than that of TiO_2, photo-generated electrons can be transferred to and accumulated in the conduction band of WO_3. Furthermore, owing to the high-crystallinity of WO_3 nanosheet, high quality of WO_3-TiO_2 and WO_3-Pt interface is obtained and recombination of photo-generated electrons and holes induced by defects can be avoided.[44] Accumulated electrons then quickly transfer to the surface of platinum nanoparticles and hence separation of electrons and holes can be promoted. Besides that, photo-generated electrons injected into Pt nanoparticles act as electron pools to

View Article Online
DOI: 10.1039/C5NJ02981C

initiate multi-electron reductions of the oxygen molecules, which further strengthen the photooxidation ability of organic substances.

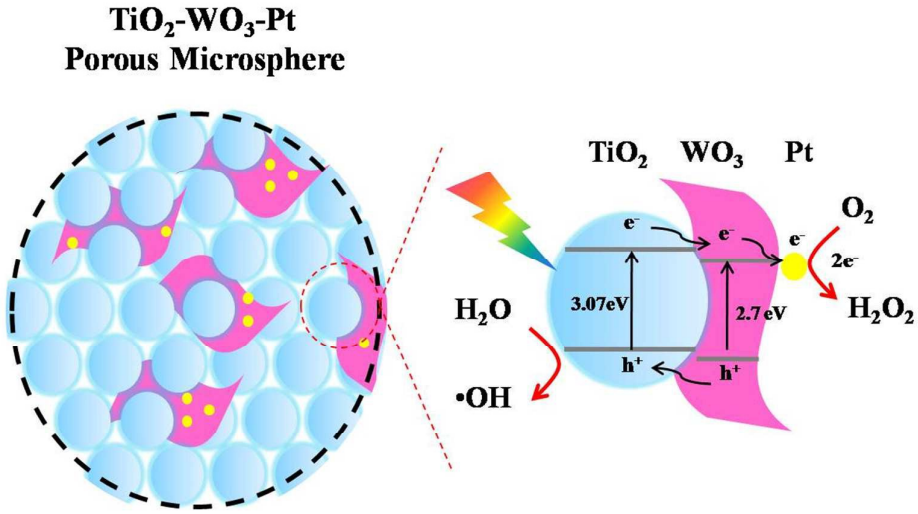

Scheme 1: Mechanism for the enhancement of photocatalytic activity of the TiO_2-WO_3-Pt multi-heterojunction.

4. Conclusions

TiO_2-WO_3-Pt multiple heterostructure porous microspheres was successfully prepared via a facile ultrasonic spray pyrolysis method. Multi-heterojunction assembled via preloading Pt nanoparticles on highly crystallized WO_3 nanosheets is found more active than that via nonselective deposition of Pt nanoparticles. The photocatalyst activity of TiO_2-WO_3-Pt multi-heterojunction (0.04 wt% of Pt) is 2.86 times higher than TiO_2-Pt heterostructure composite with the same loading amount of Pt. Furthermore, the improvement of photocatalytic performance can be confirmed by 2.66 times and 1.52 times higher in acetaldehyde degradation, and also 1.8 times and 1.03 times higher in isopropanol degradation, than that of TiO_2 and TiO_2-WO_3 composite, respectively. The as-assembled porous TiO_2-WO_3-Pt microspheres multi-heterojunction photocatalyst has a good application prospect on gas-phase photocatalytic degradation system. The method of selection of highly crystallized WO_3 nanosheets providing brilliant availability to noble metal nanoparticles for separation of photoexcited electron-hole is a good inspiration for synthesis of other multiple heterostructure photocatalyst.

View Article Online
DOI: 10.1039/C5NJ02981C

Acknowledgement:

This work was supported by the Natural Science Foundation of China (Grant Nos. 51072032, 91233204, 51372036, and 51102001), the Key Project of Chinese Ministry of Education (No 113020A), the National Basic Research Program (2012CB933703), the 111 project (No. B13013), and the International Science & Technology Cooperation Program of China (2013DFG50150), China Postdoctoral Science Foundation (2014M551156), Open Project of Key Laboratory for UV-Emitting Materials and Technology of Ministry of Education (130026505).

Notes and references:

1 A. Fujishima, X. Zhang, D. A. Tryk, *Surf. Sci. Rep.*, 2008, **63**, 515.
2 X. Chen, L. Liu, P.Y. Yu, S. S. Mao, *Science*, 2011, **331**, 746.
3 H. Chen, C. E. Nanayakkara, V. H. Grassian, *Chem. Rev.*, 2012, **112**, 5919.
4 R. Chong, J. Li, X. Zhou, Y. Ma, J. Yang, L. Huang, H. Han, F. Zhang, C. Li, *Chem. Commun.*, 2014, **50**, 165.
5 X. Qiu, M. Miyauchi, K. Sunada, M. Minoshima, M. Liu, Y. Lu, D. Li, Y. Shimodaira, Y. Hosogi, Y. Kuroda, K. Hashimoto, *ACS Nano*, 2012, **6**, 1609.
6 Y. Takahashi, T. Tatsuma, *Langmuir*, 2005, **21**, 12357.
7 K. Y. Song, M. K. Park, Y. T. Kwon, H. W. Lee, W. J. Chung, W. I. Lee, *Chem. Mater.*, 2001, **13**, 2349.
8. Y. Hu, D. Li, Y. Zheng, W. Chen, Y. He, Y. Shao, X. Fu, G. Xiao, *Appl. Catal. B-Environ.*, 2011, **104**, 30.
9 J. Wang, X. Liu, A. Yang , G. Zheng , S. Yang ,H. Wei ,Q. Zhu ,Z. Wang, *Appl. Phys. A*, 2011, **103**, 1099.
10 M. Niu, D. Cheng , D. Cao , *Sci. Rep.*, 2014, **4**, 4810.
11 Y. Chen, G. Xiao, T. Wang, F. Zhang, Y. Ma, P, Gao, C. Zhu, E. Zhang, Z. Xu, Q. Li, *Sensors Actuat. B-Chem.*, 2011, **155**, 270.
12 A.K.L.Sajjad, S.Shamaila, J.Zhang, *J. Hazard. Mater.,* 2012, **235–236**, 307
13 S. Shamaila, A.K.L. Sajjad, F. Chen, J. Zhang, *J. Colloid Interface Sci.*, 2011, **356**, 465.
14 S.A.K. Leghari, S, Sajjad, F. Chen, J. Zhang, *Chem. Eng. J.*, 2011, **166**, 906.
15 J. Tian, P. Hao, N. Wei, H. Cui, H. Liu, *ACS Catal.*, 2015, **5**, 4530.
16 R. Abe, B. Ohtani, *Photocatalysis*, 2007, **24**, 16.
17 V. Subramanian, E. Wolf, P.V. Kamat, *J. Phys. Chem. B*, 2001, **105**, 11439.
18 M.J. Height, S.E. Pratsinis, O. Mekasuwandumrong, P. Praserthdam, *Appl. Catal. B-Environ.*, 2006, **63**, 305.
19 H. Katsumata , M. Taniguchi , S. Kaneco , T. Suzuki , *Catal. Commun.*, 2013, **34**, 30.
20 R. Abe, H. Takami, N. Murakami, and B. Ohtani, *J. Am. Chem. Soc.*, 2008, **130**, 7780.

View Article Online
DOI: 10.1039/C5NJ02981C

21 L. Ni, T. Kitta, N. Kumagal, B. Ohtani, K. Hashimoto, H. Irie, *J. Ceram. Soc. JPN.*, 2013, **121**, 563.

22.X. Qiu, M. Miyauchi, H. Yu, H. Irie, K. Hashimoto, *J. Am. Chem. Soc.*, 2010, **132**, 15259.

23 M. Liu, X. Qiu, M. Miyauchi, K. Hashimoto, *Chem. Mater.*, 2011, **23**, 5282.

24 H. Yu, H. Irie, Y. Shimodaira, Y. Hosogi, Y. Kuroda, M. Miyauchi, K. Hashimoto, *J. Phys. Chem. C*, 2010, **114**, 16481.

25 H. Park, W. Choi and M. R. Hoffmann, *J. Mater. Chem.*, 2008, **18**, 2379.

26 Q. Gu, J. Long, H. Zhuang, C. Zhang, Y. Zhou and X. Wang, *Phys. Chem. Chem. Phys.*, 2014, **16**, 12521.

27 É. Karácsonyi, L. Baia, A. Dombi, V. Danciu, K. Mogyorósi, L.C. Pop, G. Kovács, V. Coşoveanu, A. Vulpoi, S. Simon, Zs. Pap, *Catal. Today*, 2013, **208**, 19.

28 C.H. Wang, X.T. Zhang, B. Yuan, Y.X. Wang, P.P. Sun, D. Wang, Y.A. Wei, Y.C. Liu, Chem. Eng. J., 2014, **237**, 29.

29 R. E. Schaak, T. E. Mallouk, *Chem. Commun.* , 2002, 706.

30 M. Sadakane, K. Sasaki, H. Kunioku, B. Obtani, R. Abe, W. Ueda, *J. Mater. Chem.*, 2010, **20**, 1811.

31 J. Yang, X. Zhang, H. Liu, C. Wang, S. Liu, P. Sun, L. Wang, Y. Liu, *Catal. Today,* 2013, **201**, 195.

32 J. Zhang, Y. Sun, Y. Yao, T. Huang, A. Yu, *J. Power Sources*, 2013, **222**, 59.

33 J. H. Bang, R. J. Helmich, K. S. Suslick, *Adv. Mater.*, 2008, **20**, 2599.

34 F. Iskandar, A. Mikrajuddin, K. Okuyama, *Nano Lett.*, 2001, **1**, 231.

35 J. H. Pan, W. I. Lee, *Chem. Mater.*, 2006, **18**, 847.

36 J. Yu, H. Yu, B. Cheng, X. Zhao, J. C. Yu, W. Ho, *J. Phys. Chem. B*, 2003, **107**, 13871.

37 C. Liu, L. Wang, Y. Tang, S. Luo, Y. Liu, S. Zhang, Y. Zeng, Y. Xu, *Appl. Catal. B-Environ.*, 2015, **164**. 1.

38 H. Kaga, K. Saito, A. Kudo, *Chem. Commun.*, 2010, **46**, 3779.

39 H. Zhou, W. Hsu, H. Duan, B. Bob, W. Yang, T. Song, C. Hsu, Y. Yang, *Energy Environ. Sci.*, 2013, **6**, 2822

40 J. C. Yu, J. Yu, W. Ho, Z. Jiang, L. Zhang, *Chem. Mater.*, 2002, **14** , 3808.

41 J. Chen, S. Shen, P. Guo, M. Wang, P. Wu, X. Wang, L. Guo, *Appl. Catal. B-Environ.,* 2014, **152**,335.

42 D. Vildozo, R. Portela, C. Ferronato, J. Chovelon, *Appl. Catal. B-Environ.*, 2011, **107**, 347.

43 C. Barakat, P. Gravejat, O. Guaitella, F. Thevenet, A. Rousseau, *Appl. Catal. B-Environ.*, 2014, **147**, 302

44 H. Kato, K. Asakura, A. Kudo, *J. Am. Chem.Soc.,* 2003, **125**, 3082.

View Article Online
DOI: 10.1039/C5NJ02981C

Graphic Abstract

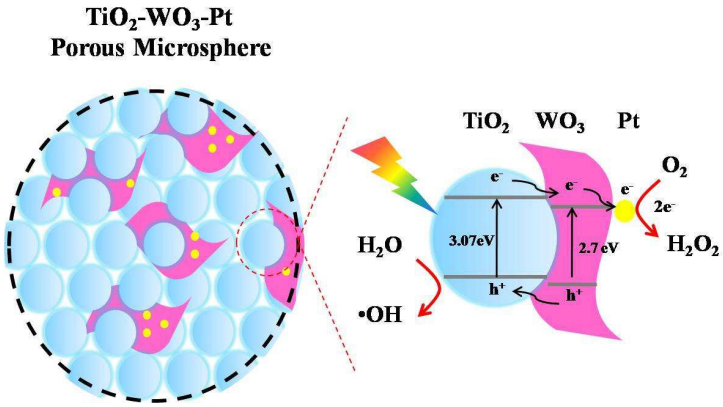

In spite of the less amount of Pt (0.04 wt%), the activity of TiO_2-WO_3-Pt multi-heterojunction is still 2.66 times and 1.52 times higher in acetaldehyde degradation tnan tnat of TiO_2 and TiO_2-WO_3 composite, respectively.